Reaction history of sapphirine granulites and a decompressional P-T path in a granulite complex from the Eastern Ghats

A MOHAN, P TRIPATHI and Y MOTOYOSHI*

Department of Geology, Banaras Hindu University, Varanasi 221 005, India
**Department of Crustal Studies, NIPR, Tokyo 173, Japan*

The sapphirine granulites from G. Madugula, Eastern Ghats preserve a variety of mineral textures and reactions. Corona and reaction textures are used in conjunction with mineral compositions to construct a sequence of metamorphic reactions describing the mineralogical evolution of sapphirine granulites. An early stage is characterized by the development of sapphirine + quartz, spinel + quartz in textural equilibrium, and possible relicts after osumilite during peak metamorphic conditions. Sapphirine/spinel crystals were later detached from quartz in the form of mineral coronas. During a subsequent sapphirine-cordierite stage, several cordierite forming reactions reflect decreasing P-T conditions. Finally during the late stage, a few samples show evidence of retrogressive hydration. Sapphirine is rather iron-rich (12.8 wt%) and the Mg number in the analysed minerals varies in the order: cordierite > phlogopite > sapphirine > orthopyroxene > spinel > garnet. P-T conditions of metamorphism have been constrained through the application of geothermobarometry and thermodynamically calibrated MAS equilibria. P-T vectors from granulite facies rocks in the G. Madugula area indicate that the rocks experienced substantial decompression (up to 3 kbar) and moderate cooling (150–200°C) subsequent to peak conditions of metamorphism (8.4 kbar, > 900°C). The decompressional P-T history of sapphirine granulites interpreted from textural features and thermobarometric estimates suggest that they may have eventually resulted from exhumation of thickened crust.

1. Introduction

Sapphirine-bearing mineral parageneses are important indicators of P-T histories and provide evidence for high temperature metamorphism in many Proterozoic granulitic terranes. Mineral associations, such as sapphirine + quartz, spinel + quartz and orthopyroxene + sillimanite ± quartz, in deep-seated granulite facies rocks from the Eastern Ghats (Grew 1982a; Lal *et al* 1987; Kamineni and Rao 1988a and b; Sengupta *et al* 1990) are of great significance because these assemblages reflect extreme cases of granulite facies metamorphism under ultra-high temperatures and high pressures (Ellis *et al* 1980; Currie and Gittins 1988; Bertrand *et al* 1992).

The geochronological information on the Eastern Ghats granulites remains inadequate at present. Ages of initial formation of the gneissic and supracrustal parent rocks of the granulites are virtually unknown, except for Sm-Nd data that gave model mantle-separation age of c. 3.0 Ga for some of the sialic material (Paul *et al* 1990). Grew and Manton (1986) obtained a c. 1.0 Ga age for sapphirine granulite from Anakapalle, E. Ghats. The effect and the relationship of the younger 1.0 Ga event on the older granulites is not fully understood. However, recent isotopic studies indicate that granulite overprinting and reworking possibly occurred in the E. Ghats at c. 1.0 Ga (Aftalion *et al* 1988; Grew and Manton 1986; Paul *et al* 1990). Due to poorly constrained isotopic studies

Keywords. Sapphirine granulites; corona textures; geothermobarometry; decompression; Eastern Ghats.

Proc. Indian Acad. Sci. (Earth Planet. Sci.), **106**, No. 3, September 1997, pp. 115–129

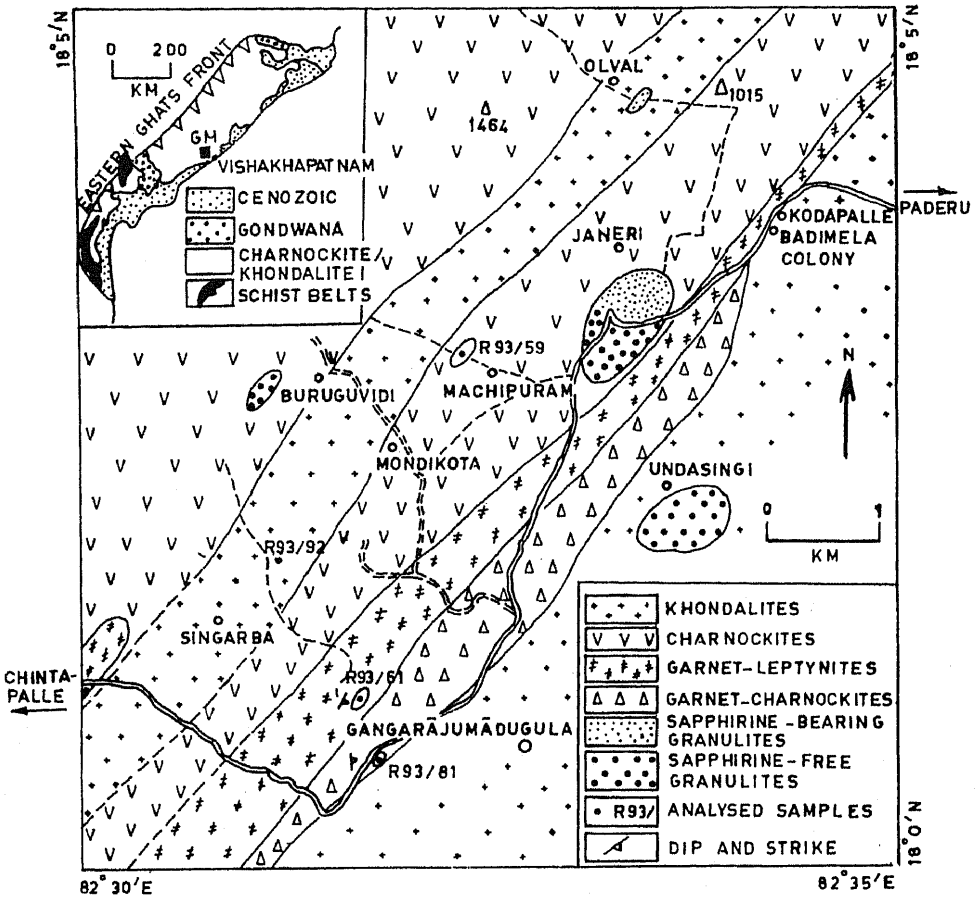

Figure 1. Geological sketch map of the study area showing major rock types and sample locations. Inset shows generalized geological map of the E. Ghats belt and location of the G. Madugula area.

in the E. Ghats, the present ages should be interpreted with caution.

In this paper we report a new sapphirine-spinel-quartz association from G. Madugula and describe a decompressional history that has been interpreted using coronas, reaction textures and geothermobarometry. The discussion on P-T path has been extended further to provide information on the tectonic mechanism related to the metamorphic evolution of E. Ghats granulites.

2. Field aspects

Sapphirine-bearing rocks occur as enclaves within the granulite facies garnetiferous charnockites close to the contact with khondalite near Gangaraja Madugula, located about 120 km north-west of Visakhapatnam town, Andhra Pradesh (figure 1). These rocks contain sapphirine, orthopyroxene, sillimanite, cordierite, garnet, spinel, quartz, phlogopite and k-feldspar in a variety of assemblages. Some associations are characterized by the stable association of spinel + quartz and sapphirine + quartz.

3. Petrography

Sapphirine-bearing granulites are texturally characterized by sharp contacts between sapphirine-quartz and spinel-quartz. Besides, these rocks also contain orthopyroxene, sillimanite, cordierite, garnet, phlogopite and k-feldspar in a variety of assemblages. Minor amounts of zircon, rutile, apatite and ilmenite are also present. Occasionally, corundum grains are associated with spinel and ilmenohematite, but never in contact with quartz. Thin hematite lamellae were observed in reflected light studies.

Mineral reactions inferred from reaction coronas and symplectitic intergrowths can be subdivided into distinct stages.

3.1 *Early stage*

Early formed minerals were partially used up in the formation of later assemblages; the early assemblages are, therefore, incomplete. The textural history of the early stage is characterized by the development of sapphirine + quartz, spinel + quartz in textural equilibrium (Plate 1A) and very fine grained symplectites of k-feldspar, cordierite, quartz and orthopyroxene

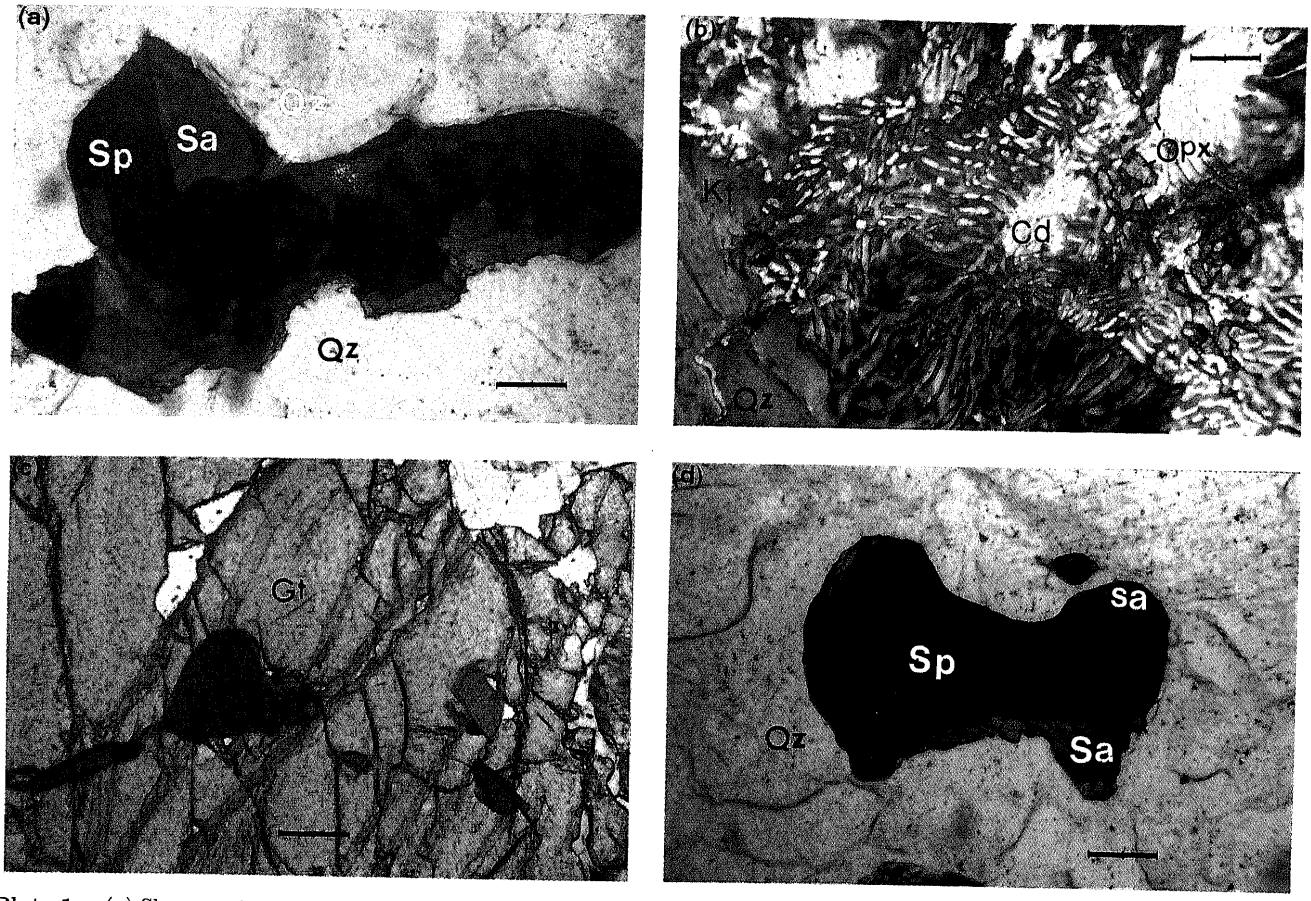

Plate 1. (a) Sharp grain contacts of sapphirine + quartz and spinel + quartz; scale bar = 0.1 mm. (b) Very fine symplectites of orthopyroxene-cordierite-K-feldspar-quartz as possible relicts after osumilite; scale bar = 0.1 mm. (c) Inclusions of oval shaped prograde biotite within garnet blast; scale bar = 0.1 mm; (d) Sapphirine rim around coarse spinel crystal, scale bar = 0.1 mm.

(Plate 1B), which we interpret as a breakdown product of osumilite (Berg and Wheeler 1976). Identical textures have been described in the granulite facies rocks from Antarctica where they demonstrably formed by the breakdown of osumilite (Ellis *et al* 1980; Grew 1982b) and also from S. India (Grew 1982a; Lal *et al* 1987).

Corroded prograde biotites (high Ti content) showing crude alignment within porphyroblasts of garnet (Plate 1C), and coarse prisms of orthopyroxene (high Al_2O_3) are interpreted as part of the primary paragenesis. In places, blocky sillimanite defines the foliation. Coarse prisms of sapphirine are strongly pleochroic; (X = pale yellow, Y = greenish blue and Z = deep sapphire blue). These assemblages, as supported by textural evidence, make up the early recognizable stable assemblage prior to the growth of coronas and symplectites.

3.2 *Corona stage*

Textural relationships such as corona of sapphirine around spinel (Plate 1D) suggest that the former is a late phase. A composite texture showing coronal development of sillimanite and orthopyroxene over the sapphirine and spinel contacting quartz is observed. Sapphirine with partial rim of sillimanite is mantled by orthopyroxene (Plate 2A). Elsewhere, sapphirine is successively rimmed by sillimanite and garnet in quartz matrix. Spinel is commonly surrounded by complex coronas involving garnet and sillimanite; e.g., spinel is separated from quartz by a corona of sillimanite + orthopyroxene (Plate 2B), orthopyroxene + sapphirine (Plate 2C) and sillimanite + garnet (Plate 2D) etc. Also spinel is partly rimmed by sapphirine that is enveloped within a coarse garnet blast. In some samples, spinel displays partial rimming of sapphirine, followed by sillimanite that is enclosed within garnet porphyroblast (Plate 3A). Corundum crystals are enclosed in exsolved magnetite-spinel (Plate 3D) indicating prevalence of oxidizing state. Most likely the coronas were formed simultaneously under high fO_2 conditions.

3.3 *Cordierite stage*

During this stage we find development of tiny lumps of garnet, orthopyroxene or symplectitic intergrowths of spinel-cordierite, orthopyroxene-cordierite, in

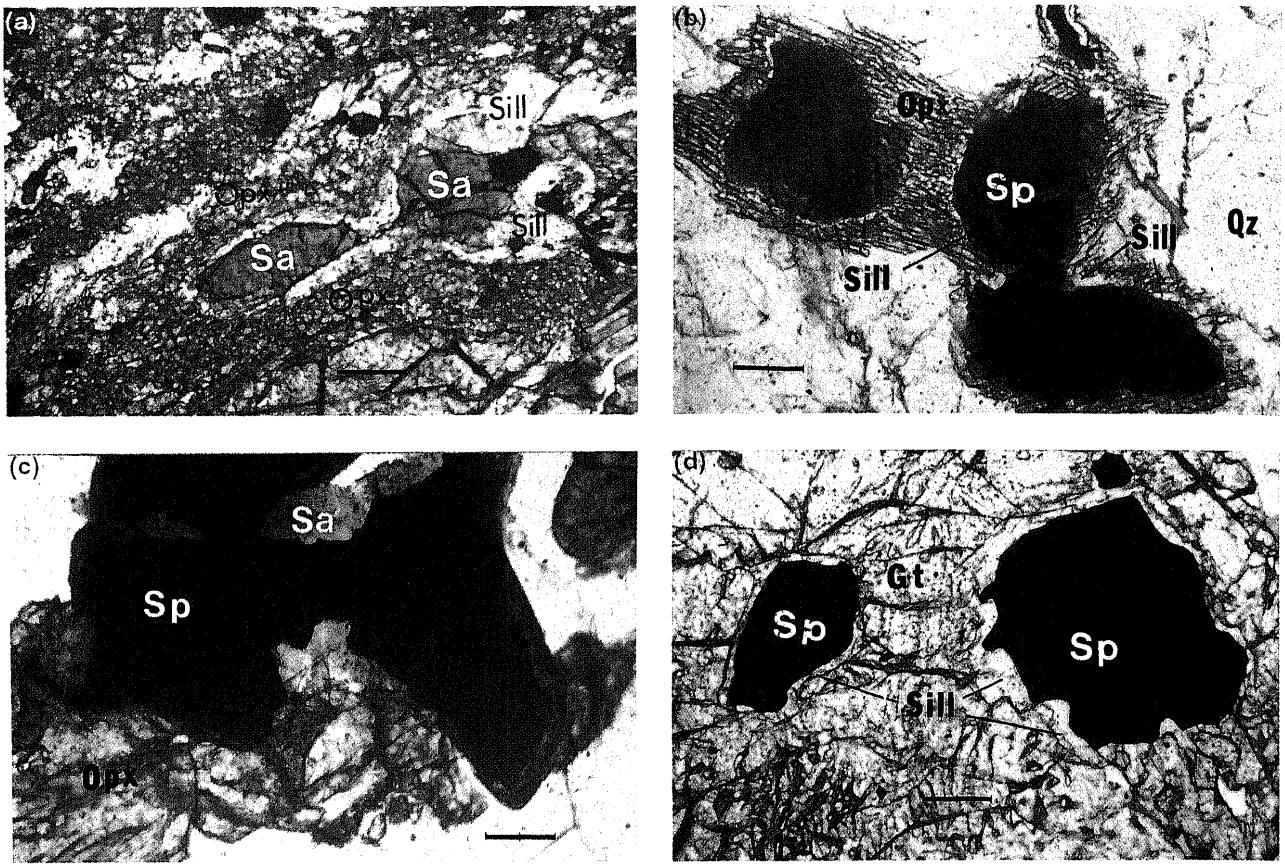

Plate 2. (**a**) Sapphirine blasts with a thin rim of sillimanite mantled by orthopyroxene; scale bar = 0.1 mm. (**b**) Megacryst of spinel successively rimmed by sillimanite and orthopyroxene, scale bar = 0.1 mm. (**c**) Corona of sapphirine and orthopyroxene around coarse spinel; scale bar = 0.1 mm. (**d**) Coarse spinel with narrow sillimanite rim, enclosed within garnet porphyroblast; scale bar = 0.1 mm.

contrast with the coarse crystals that typify the earlier stages.

Cordierite is the major product in these overprinting textures. Thin sections reveal cordierite rims and/or overgrowths around sapphirine (Plate 3B) and spinel. Garnet is detached from quartz by orthopyroxene + cordierite-rich domain. Cordierite moats are observed between orthopyroxene-sillimanite segregates, and also between sillimanite and resorbed garnet. Symplectitic intergrowth of spinel and cordierite around sapphirine is another textural feature. The symplectites of tiny nodules of garnet intergrowths with quartz surround earlier grown orthopyroxene and garnet blasts (Plate 3C).

3.4 *Hydration stage*

During this stage, a few samples show evidence of retrogressive hydration where biotite or biotite + quartz symplectites replace orthopyroxene, garnet and cordierite. Biotite-quartz symplectites also surround garnet-quartz symplectites (Plate 3C) implying that the latter developed prior to biotite-quartz symplectites

4. Mineral chemistry

Electron microprobe analyses were carried out on a JEOL, JCXA-733 at NIPR, Tokyo operated at an acceleration voltage of 15 kV and a specimen current of 0.014 μA. Natural minerals (natural albite for Na_2O, wollastonite for CaO) and synthesized oxides for the rest of oxides were used as standards. On-line data reduction utilized the Bence and Albee correction program. Representative analytical data are given in table 1(a–e).

Sapphirines are fairly iron-rich (12.18 wt% FeO) and highly aluminous (c.60 wt% Al_2O_3), they plot close to 7:9:3 end-member [(MgFe)O: R_2O_3: SiO_2, in mol.] due to (Mg, Fe^{2+}) + Si = 2 (Al, Fe^{3+}, Cr) substitution (Higgins *et al* 1979). Sapphirines containing higher Al_2O_3 (up to 64 wt%) fall within the peraluminous area beyond 7:9:3 composition (figure 2). The sapphirine analyses are calculated on the basis of 20 oxygen. With all iron as Fe^{2+}, cation totals generally exceed 14.00, implying that some Fe^{3+} is present. Ferric iron (0.33–0.40) is present in all analyses based on the ferrous-ferric recalculation scheme described by Higgins *et al* (1979). Higher

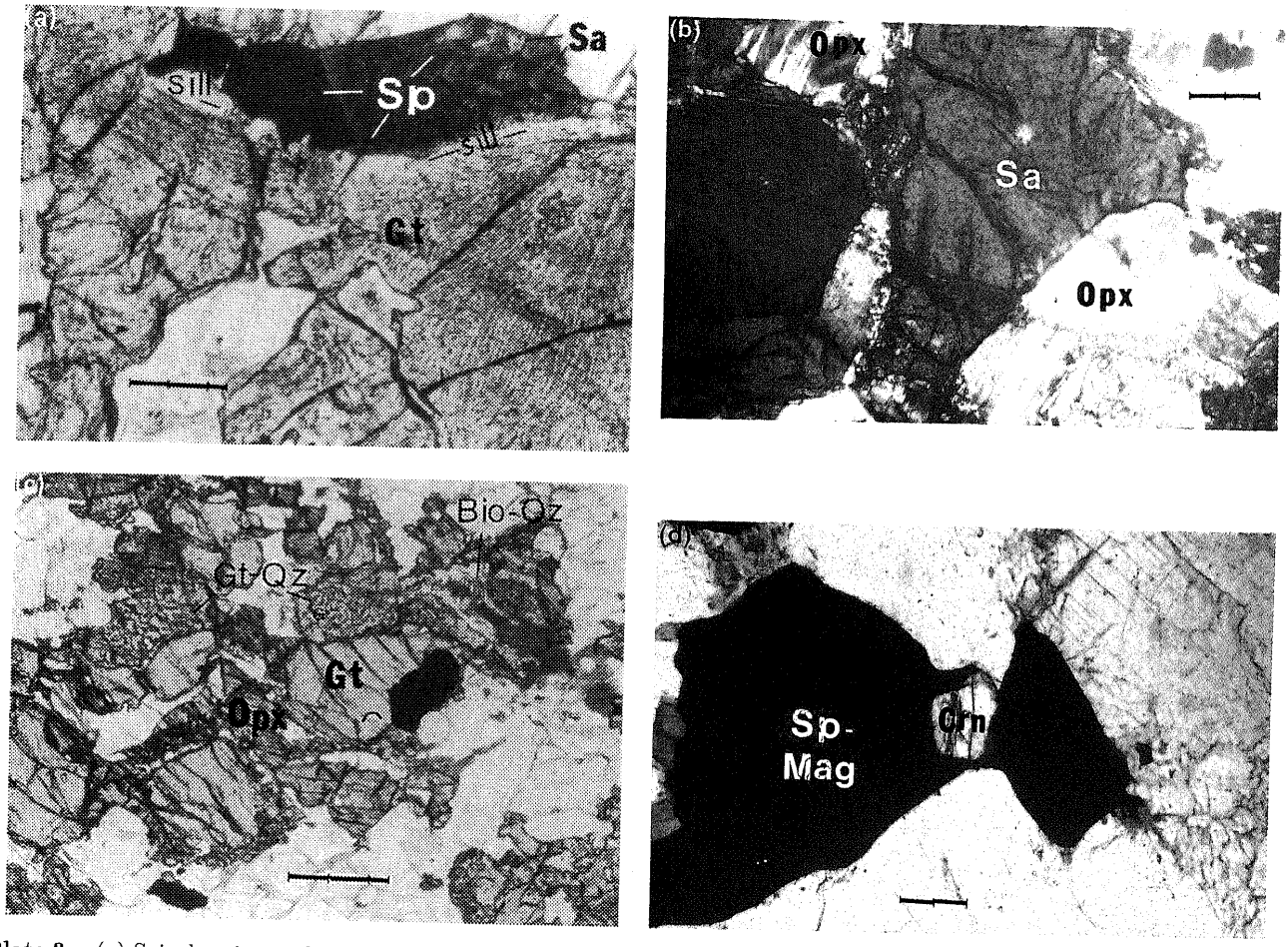

Plate 3. (**a**) Spinel grain partly rimmed by sapphirine and sillimanite within garnet blast; scale bar = 0.5 mm. (**b**) Sapphirine blast engulfed by cordierite; scale bar = 0.1 mm. (**c**) Tiny nodules of garnet intergrown with quartz surround earlier orthopyroxene and garnet crystals. Late biotite-quartz symplectites surround garnet-quartz symplectites; scale bar = 0.5 mm. (**d**) Corundum crystal trapped in exsolved magnetite-spinel megacryst; scale bar = 0.1 mm.

trivalent iron is present when sapphirine is in textural equilibrium with quartz. Cr_2O_3 content is very low.

The $X_{Mg}[= Mg/(Fe^{2+} + Mg)]$ ranges from 0.77–0.81. Compositional zoning in individual crystals is generally absent. Composition variations are noted among grains from different reaction coronas. Sapphirine enclosed by garnet has higher X_{Mg} (0.81).

Cordierite is systematically richer in magnesium than coexisting phases (X_{Mg}: 0.85–0.88). In this mineral no significant zoning was detected. The low oxide totals of some cordierites could suggest the presence of volatiles trapped in their crystal structure (Armbruster and Bloss 1980).

Spinels are generally dominated by the solid solutions of Mg spinel-hercynite and magnetite. The spinel grains contain minor ZnO (< 1 wt%) and Cr_2O_3 (up to 0.33 wt%); yet this Cr_2O_3 percentage is higher than associated sapphirine. Calculation of Fe^{3+}, based on stoichiometric considerations (Bohlen and Essene 1977) indicate a significant amount of trivalent iron (0.32–0.50 p.f.u.). X_{Mg} values of spinel, recalculated after extraction of Fe^{3+}, are in the range 0.47–0.62.

Orthopyroxenes have cation totals close to 4.00 per 6 oxygens, implying that little Fe^{3+} is present based on the method of Hamm and Vieten (1971). Variations in Al_2O_3 content from grain to grain in the same sample were measured. There is a systematic decrease in Al_2O_3 from core to rim and the X_{Mg} ranges from 0.68 to 0.72. A decrease in Al_2O_3 from core to rim is usually concomitant with increasing MgO, SiO_2 and FeO (Arima and Barnett 1984). Low mobility of alumina possibly causes higher Al_2O_3 in the cores. We do find orthopyroxenes with Al_2O_3 10.1 wt%. That does indicate high temperature and shows that such grains failed to reequilibriate. Two generations of orthopyroxene also occur in the same thin section with different X_{Al} c.10% and c.7 wt%. That is significant and shows the rocks were once hot (850–950°C, see discussion on *P-T* conditions). Higher contents of Al_2O_3 (up to 13 wt%) in orthopyroxenes reported from granulitic terranes are summarized in table 2 for comparison. Lower X_{Mg} (c. 0.59) and alumina content (c. 2.0 wt%) is typical in charnockites.

Garnets are mainly almandine (48.7–61.9%)-pyrope (27.8–47.6 mol%) solid solutions with low

Table 1(a). *Selected microprobe analyses.*

	GARNET (24 oxygen basis)							
Sample no.	R93/59	R93/59	R93/92	R93/92	R93/92	R93/80	R93/80	R93/80
Spot Oxide	4C	6C	1R	2I	3C	6C	7R	24R
SiO_2	39.94	39.93	38.70	39.02	38.27	39.93	40.04	39.55
TiO_2	—	—	0.06	0.03	—	0.04	0.04	—
Al_2O_3	22.42	22.39	21.63	21.67	20.52	22.60	22.45	22.51
Cr_2O_3	—	0.01	0.03	0.01	—	—	—	0.06
FeO*	26.64	25.85	28.99	29.08	29.35	24.42	24.22	23.68
MnO	0.97	0.99	0.71	0.89	0.79	0.48	0.56	0.57
MgO	11.25	11.58	7.45	7.38	7.51	12.90	12.85	12.99
CaO	0.73	0.67	3.46	2.97	2.90	0.88	0.60	0.96
Total	101.95	101.42	101.00	100.98	99.34	101.25	100.76	100.32
Si	5.985	5.992	5.974	6.014	6.029	5.956	5.992	5.945
Ti	—	—	0.007	0.003	—	0.004	0.005	—
Al	3.960	3.962	3.937	3.938	3.811	3.974	3.961	3.989
Cr	—	0.002	0.003	0.001	—	—	—	0.007
Fe*	3.338	3.244	3.743	3.748	3.867	3.046	3.031	2.977
Mn	0.122	0.125	0.093	0.116	0.105	0.061	0.071	0.073
Mg	2.511	2.590	1.713	1.696	1.763	2.868	2.866	2.911
Ca	0.118	0.108	0.572	0.491	0.490	0.141	0.096	0.154
X_{Mg}	0.429	0.444	0.314	0.312	0.313	0.485	0.486	0.494
Pyrope	41.2	42.7	27.8	28.1	28.3	46.9	47.3	47.6
Grossular	1.9	1.8	9.4	8.1	7.9	2.4	1.6	2.5
Almandine	54.8	53.5	61.3	61.9	62.1	49.8	49.9	48.7
Spessartine	2.1	2.0	1.5	1.4	1.7	0.9	1.2	1.2

*Total iron as FeO or Fe^{2+}.
R 93/59, 61, 80: Sapphirine granulites.
R 93/92: Garnet charnockite.

MnO and CaO content (< 2 and 3 mol% spessartine and grossular respectively). On the basis of stoichiometric considerations, this phase does not contain any andradite component. Garnet grains throughout the sample are homogeneous in composition. Garnets have lower X_{Mg} (0.31) in charnockites and garnet-quartz symplectites than the sapphirine-garnet (X_{Mg} : 0.43–0.50)-bearing assemblages.

Biotites with high TiO_2-content (4.46 wt%) are characteristic of sapphirine-bearing mineral assemblages. Phlogopite from sapphirine-bearing rocks invariably has higher X_{Mg} (0.83–0.87) than those from charnockite (0.78). Biotite in some samples is retrograde.

In **Sillimanite and Corundum** the only impurity detected was iron (0.94–1.0 per cent Fe_2O_3 in sillimanite, 0.93–1.33 per cent in corundum); Mn_2O_3 was negligible. High Fe_2O_3 content of sillimanite is consistent with the high Fe^{3+} content of associated sapphirine and spinel.

Orthoclase content in **alkali feldspar** ranges from 81–89%. **Plagioclase** in charnockites ranges in composition from An_{44}-An_{47}.

Ilmenite is essentially pure. Minor rutile, apatite, zircon and magnetite may be present as well. The X_{Mg} values among various minerals are as follows: cordierite > phlogopite > sapphirine > orthopyroxene > spinel > garnet.

5. Interpretation of mineral textures and reaction history

In this section an attempt is made to deduce the sequence of metamorphic reactions describing the mineralogical evolution of sapphirine granulites utilizing the mineral textures and compositions. The observed textures are obviously the result of a complex reaction history. These reactions inferred from textural relationships have been verified in the chemographic configuration depicted by (MgO + FeO)-Al_2O_3-SiO_2 diagram (figure 3).

5.1 *Corona forming reactions*

The textures exhibiting a continuous or partial rim of sapphirine around spinel provides evidence for the following continuous reaction:

$$\text{Spinel} + \text{quartz} = \text{sapphirine}_{2:2:1}. \quad (1)$$

A corona of sapphirine + orthopyroxene separating spinel and quartz may have formed by the continuous

Table 1(b).

	SAPPHIRINE (14 cation basis)						SPINEL (3 cation basis)					
Sample no Spot Oxide	R93/61 1C	R93/61 2NR	R93/61 3C	R93/59 2R	R93/80 1C	R93/80 2R	R93/59 1R	R93/59 11C	R93/80 3R	R93/80 4C	R93/61 7C	R93/61 18R
SiO_2	12.97	13.39	13.31	10.99	11.31	11.66	1.54	0.03	—	0.04	—	—
TiO_2	0.06	0.06	0.07	0.05	0.05	0.08	—	0.02	0.03	—	0.02	0.01
Al_2O_3	60.03	59.09	59.48	63.71	62.90	62.87	58.39	48.88	62.05	62.05	61.38	62.05
Cr_2O_3	0.03	0.08	0.06	—	0.07	0.04	—	—	0.19	0.21	0.14	0.33
FeO*	12.02	12.18	11.82	10.56	10.28	10.07	26.40	38.87	24.58	24.56	25.48	25.30
MnO	0.13	0.15	0.10	0.05	0.05	0.07	0.07	0.07	—	0.05	0.14	0.12
MgO	15.18	15.44	15.28	14.71	14.81	15.38	12.43	12.77	13.49	12.51	11.42	11.34
CaO	0.04	0.03	0.01	0.02	0.02	0.02	—	—	0.02	—	—	0.02
Na_2O	—	—	0.02	—	—	0.03	—	—	0.04	0.05	0.03	0.03
K_2O	—	—	0.01	0.02	0.01	—	—	—	—	0.01	—	—
ZnO	0.20	0.06	0.06	—	0.02	—	0.18	0.18	0.47	0.50	0.90	0.61
Total	100.66	100.48	100.12	100.11	99.52	100.22	99.01	100.82	100.87	99.98	99.51	99.81
Si	1.556	1.609	1.600	1.317	1.361	1.391	0.042	0.001	—	0.001	—	—
Ti	0.006	0.005	0.006	0.004	0.005	0.007	—	—	0.001	—	—	—
Al	8.484	8.368	8.436	8.988	8.925	8.842	1.857	1.580	1.918	1.941	1.944	1.958
Cr	0.003	0.008	0.005	—	0.007	0.004	—	—	0.004	0.005	0.003	0.007
Fe^{2+}	0.816	0.828	0.843	0.686	0.694	0.646	0.361	0.321	0.438	0.425	0.477	0.503
Fe^{3+}	0.390	0.396	0.347	0.371	0.335	0.359	0.235	0.570	0.101	0.970	0.095	0.063
Mn	0.013	0.015	0.010	0.005	0.005	0.007	0.002	0.002	—	0.001	0.003	0.003
Mg	2.711	2.764	2.740	2.623	2.656	2.734	0.500	0.522	0.527	0.495	0.457	0.452
Ca	0.005	0.003	0.001	0.003	0.003	0.003	—	—	—	—	—	0.001
Na	—	—	0.005	—	—	0.008	—	—	0.002	0.003	0.001	0.001
K	—	—	0.002	0.003	0.001	—	—	—	—	—	—	—
Zn	0.018	0.005	0.005	—	0.002	—	0.003	0.004	0.008	0.010	0.018	0.012
X_{Mg}	0.769	0.770	0.765	0.793	0.792	0.809	0.581	0.620	0.546	0.538	0.489	0.473

* Total iron as FeO.

Table 1(c).

	ORTHOPYROXENE (4 cation basis)									
Sample no. Spot Oxide	R93/59 27C	R93/59 30C	R93/80 17C	R93/80 18R	R93/80 20R	R93/92 8R	R93/92 9C	R93/61 10C	R93/61 11R	R93/59 26C
SiO_2	48.02	48.69	48.61	49.01	49.26	50.81	51.12	47.73	47.87	48.32
TiO_2	0.13	0.05	0.12	0.07	—	0.02	0.04	0.13	0.08	0.15
Al_2O_3	7.80	8.13	8.80	8.31	7.57	2.21	1.91	10.09	8.86	8.54
Cr_2O_3	0.01	0.01	0.06	0.01	—	—	0.01	—	0.02	0.02
FeO*	19.68	19.65	19.39	19.64	19.09	26.82	26.34	20.38	20.52	19.02
MnO	0.21	0.19	0.18	0.15	0.13	0.22	0.24	0.27	0.30	0.20
MgO	23.22	23.17	22.90	23.21	23.67	19.98	20.08	21.56	22.26	22.88
CaO	0.03	0.05	0.05	0.04	0.05	0.31	0.32	0.07	0.05	0.07
Na_2O	—	0.02	0.05	0.02	—	0.02	0.01	0.02	—	0.02
K_2O	0.01	0.01	0.01	0.01	—	0.01	0.03	—	0.01	—
Total	99.11	99.97	100.17	110.47	99.77	100.40	100.10	100.23	99.97	99.22
Si	1.769	1.778	1.771	1.781	1.798	1.926	1.927	1.748	1.757	1.777
Ti	0.004	0.001	0.002	0.002	—	0.001	0.001	0.004	0.002	0.004
Al	0.339	0.350	0.378	0.356	0.326	0.099	0.085	0.436	0.384	0.370
Cr	—	—	0.002	—	—	—	—	—	0.001	0.001
Fe^{2+}	0.491	0.507	0.513	0.518	0.505	0.801	0.771	0.560	0.531	0.517
Fe^{3+}	0.115	0.093	0.078	0.079	0.078	0.049	0.059	0.063	0.099	0.068
Mn	0.007	0.006	0.006	0.005	0.004	0.007	0.008	0.009	0.009	0.006
Mg	1.275	1.261	1.243	1.257	1.288	1.100	1.128	1.177	1.217	1.254
Ca	0.001	0.002	0.002	0.002	0.002	0.012	0.013	0.003	0.001	0.003
Na	—	0.001	0.004	0.001	—	0.001	0.001	0.002	—	0.001
K	—	—	—	—	—	0.001	0.001	—	0.010	—
X_{Mg}	0.722	0.713	0.708	0.708	0.718	0.580	0.594	0.678	0.696	0.708

* Total iron as FeO.

Table 1(d).

	CORDIERITE (18 oxygen basis)					BIOTITE (22 oxygen basis)				
Sample no. Spot Oxide	R93/59 18R	R93/59 19C	R93/59 21R	R93/80 12C	R93/80 13C	R93/61 13C	R93/61 14R	R93/80 15C	R93/61 20C	R93/92 14R
SiO_2	49.76	49.58	48.89	49.23	49.26	49.26	49.11	39.08	39.22	39.30
TiO_2	0.01	0.01	—	0.01	—	—	0.01	3.99	4.46	4.46
Al_2O_3	33.68	33.70	33.67	32.86	33.16	33.05	33.48	14.22	12.97	12.54
Cr_2O_3	—	—	—	0.01	—	—	—	0.01	0.03	—
FeO*	3.35	3.17	3.03	3.50	3.42	3.97	3.71	5.90	7.49	9.60
MnO	0.07	0.05	0.05	0.02	0.05	0.08	0.10	—	—	—
MgO	12.04	11.76	12.05	12.04	11.61	11.74	11.62	21.65	20.50	19.09
CaO	—	0.05	0.03	—	0.01	0.02	0.04	0.07	0.02	0.01
Na_2O	0.04	0.02	0.02	0.06	—	0.03	—	0.15	0.20	0.07
K_2O	0.01	—	—	0.03	0.01	0.02	0.02	10.19	10.37	10.09
Total	98.96	98.34	97.74	97.76	97.52	98.17	98.09	95.26	95.26	95.16
Si	4.977	4.984	4.946	4.990	4.999	4.984	4.965	5.613	5.683	5.745
Ti	0.001	0.001	—	0.001	—	—	0.001	0.431	0.486	0.490
Al	3.972	3.993	4.016	3.927	3.967	3.941	3.990	2.408	2.216	2.162
Cr	—	—	—	0.001	—	—	—	0.001	0.004	—
Fe	0.280	0.266	0.256	0.297	0.290	0.336	0.314	0.709	0.908	1.174
Mn	0.006	0.005	0.005	0.002	0.004	0.007	0.008	—	—	—
Mg	1.795	1.761	1.817	1.818	1.756	1.770	1.751	4.634	4.427	4.160
Ca	—	0.005	0.003	—	0.001	0.002	0.005	0.003	0.003	0.001
Na	0.008	0.004	0.004	0.011	—	0.005	—	0.043	0.056	0.019
K	0.001	—	—	0.004	0.001	0.002	0.003	1.867	1.918	1.881
X_{Mg}	0.865	0.869	0.877	0.860	0.858	0.845	0.848	0.867	0.830	0.780

* Total iron as FeO or Fe^{2+}

Table 1(e).

	SILLIMANITE(1-0)		ILMENITE(4-Catns.)		CORUNDUM(3-0)		PLAGIOCLASE(32-0)		K-FELDSPAR(32-0)	
Sample no.	R93/59	R93/59	R93/92	R93/61	R93/61	R93/59	R93/92	R93/92	R93/80	R93/59
Spot Oxide	14C	24C	11C	19C	17C	10C	7R	13R	16R	33R
SiO_2	36.74	36.71	—	—	0.05	0.04	57.27	57.69	65.13	64.21
TiO_2	—	0.03	49.31	41.44	0.02	—	—	—	—	64.21
Al_2O_3	61.65	62.35	—	0.03	100.85	100.06	27.49	27.22	18.34	18.74
Cr_2O_3	—	—	0.03	0.01	0.02	—	0.04	0.05	—	0.03
FeO*	—	—	49.80	56.76	0.93	1.33	0.02	0.17	0.02	0.06
Fe_2O_3	1.00	0.94	—	—	0.93	1.33	—	—	—	—
MnO	—	0.01	0.14	0.36	0.05	0.01	—	0.02	—	—
MgO	—	0.02	1.11	0.81	—	0.01	—	—	—	—
CaO	0.03	—	0.02	0.03	0.01	—	9.46	9.44	0.10	0.12
Na_2O	—	—	0.04	—	—	0.01	5.72	6.36	1.91	1.25
K_2O	0.01	—	0.01	—	—	—	0.25	0.32	12.99	15.32
ZnO	0.09	0.19	0.05	0.05	0.05	0.02	0.03	0.10	—	—
Total	99.52	100.25	100.51	99.52	101.98	101.48	100.28	101.37	98.49	94.75
Si	4.006	3.864	—	—	0.001	0.001	2.558	2.560	3.013	2.973
Ti	—	0.003	0.945	0.839	—	—	—	—	—	0.001
Al	7.924	8.110	—	0.001	1.989	1.986	1.448	1.424	1.000	1.023
Cr	—	—	0.001	—	—	—	0.001	0.002	—	0.001
Fe	—	—	1.061	1.278	—	—	0.001	0.006	0.001	0.002
Fe^{3+}	0.091	0.083	—	—	0.013	0.019	—	—	—	—
Mn	—	0.001	0.003	0.008	0.001	—	—	0.001	—	—
Mg	—	0.003	0.042	0.032	—	—	—	—	—	—
Ca	0.003	—	0.001	0.001	—	—	0.453	0.449	0.005	0.006
Na	—	—	0.002	—	—	—	0.496	0.547	0.171	0.112
K	0.002	—	—	—	—	—	0.014	0.018	0.767	0.905
Zn	0.007	0.014	0.001	0.001	0.001	—	0.001	0.003	—	—
X_{Ca}	—	—	—	—	—	—	0.470	0.443	—	—
X_K	—	—	—	—	—	—	—	—	0.813	0.885

* Total iron as FeO or Fe^{2+}.

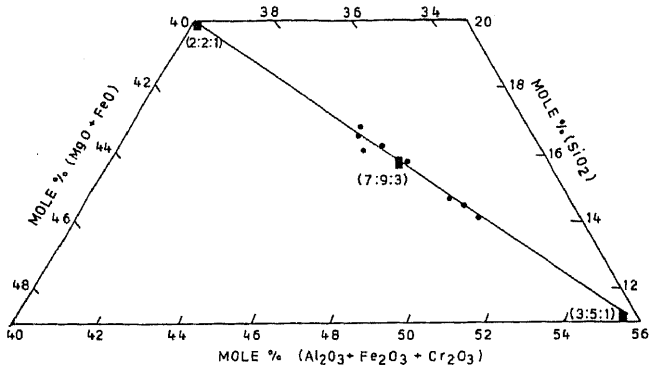

Figure 2. Plot of sapphirine compositions from present study in portion of the $(MgO + FeO)$-$(Al_2O_3 + Fe_2O_3 + Cr_2O_3)$-$(SiO_2)$ diagram. The ratios 2:2:1, 7:9:3 and 3:5:1 refer to the mole proportion of (Mg, Fe) O: R_2O_3 : SiO_2.

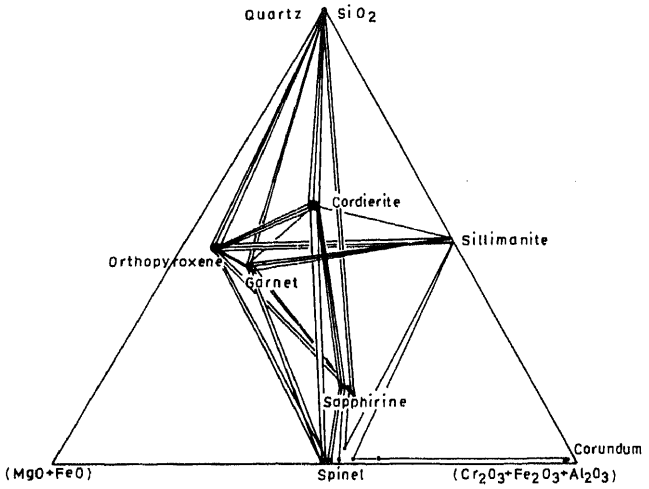

Figure 3. Chemographic relationships among phases in the system (Mg, Fe) 0-$(Al_2O_3 + Fe_2O_3 + Cr_2O_3)$-$SiO_2$.

Fe^{2+}-Mg reaction:

$$\text{Spinel} + \text{quartz} = \text{sapphirine}_{7:9:3} + \text{orthopyroxene}. \quad (2)$$

Intersecting spinel-quartz and sapphirine-orthopyroxene tie-lines further attest to the reaction (2).

The composite texture in the corona type sapphirine-spinel-sillimanite-orthopyroxene indicates a discontinuous reaction:

$$\text{Spinel} + \text{sapphirine} + \text{quartz} = \text{orthopyroxene} + \text{sillimanite}. \quad (3)$$

The analysed spinel has low Zn and high Fe^{3+} content. In low-Zn bulk composition, spinel-quartz-orthopyroxene-sillimanite association is restricted to a very narrow zone in FMAS (high fO_2) grid of Hensen 1986 ($> 900°C$, ~ 9 kbar), which provides distinct evidence for high temperature metamorphism. Orthopyroxene + sillimanite of the product assemblage, with two out of the three reactant minerals in the reaction (3) make up divariant assemblages for the Fe^{2+}-Mg continuous reactions:

$$\text{Spinel} + \text{quartz} = \text{orthopyroxene} + \text{sillimanite}. \quad (4)$$

$$\text{Sapphirine} + \text{quartz} = \text{orthopyroxene} + \text{sillimanite}. \quad (5)$$

For both these reactions (4) and (5), textural evidence such as sillimanite rims around spinel and sapphirine mantled by orthopyroxene were observed. Hensen (1986) suggested a positive dP/dT slope for reaction (5) where orthopyroxene + sillimanite coexist at high pressure and low temperature side of this cooling reaction. Reaction (4) has been experimentally investigated by Chatterjee and Schreyer (1972).

In garnet-bearing samples, spinel included within the garnet blasts, is detached by a thin rim of sillimanite via reaction:

$$\text{Spinel} + \text{quartz} = \text{garnet} + \text{sillimanite}. \quad (6)$$

Crossing of spinel-quartz and garnet-sillimanite joins also attest to reaction (6). Successive rims of sillimanite and garnet on sapphirine suggest the following reaction:

$$\text{Sapphirine} + \text{quartz} = \text{garnet} + \text{sillimanite}. \quad (7)$$

Intersecting tie-lines involving sapphirine + quartz and garnet + sillimanite in (F+M)AS diagram supports reaction (7).

A rim of sapphirine over spinel enclosed within garnet crystal suggests that spinel becomes incompatible with quartz that is related through the reaction:

$$\text{Spinel} + \text{quartz} = \text{sapphirine} + \text{garnet}. \quad (8)$$

The development of sapphirine-sillimanite-spinel-garnet corona is related to reaction (9) where texturally

Table 2. *Al_2O_3 content (wt%) of orthopyroxene.*

Locality	Al_2O_3 wt%	Reference
Enderby Land, Antarctica	11.3	Ellis *et al* 1980
Wilson Laka, Labrador	10.71	Currie and Gittins 1988
Paderu, E. Ghats	10.4	Lal *et al* 1987
Ganguvarpatti, T.N.	10.7	Mohan and Windley 1993
Gruf Complex, Alps	9–11	Droop and Bucher-Nurminen 1984
Enderby Land, Antarctica	8–9.5	Harley *et al* 1990
In Ouzzal, Algeria	11.81	Bertrand *et al* 1992
Anantgiri, E. Ghats	7.15–9.09	Sengupta *et al* 1990
Paderu, E. Ghats	13.18	Grew 1982a

one of the reactant phase (spinel) is separated from the remaining two reactants (garnet and sillimanite) by a product mineral (sapphirine).

$$\text{Spinel} + \text{garnet} + \text{sillimanite} = \text{sapphirine}. \quad (9)$$

The compositional plot of sapphirine within the three-phase field of spinel-garnet-sillimanite also attests to formation of sapphirine according to reaction (9).

Some of the observed corona textures interpreted to indicate cooling, may also result from change in fO_2 conditions which is apparently related to exsolution phenomenon. These textures could also form during decompression, but that decompression should have been associated with significant cooling as well.

5.2 *Cordierite-forming reactions*

During a subsequent stage several possible cordierite-forming reactions, for which textural evidence exist, reflect decreasing P-T conditions. The presence of a rim of cordierite over sapphirine and spinel suggests the following reactions:

$$\text{Sapphirine}_{2:2:1} + \text{quartz} = \text{cordierite}. \quad (10)$$

$$\text{and Spinel} + \text{quartz} = \text{cordierite}. \quad (11)$$

In the MAS system, the equilibrium (10) has almost flat $\mathrm{d}P/\mathrm{d}T$ slope (Newton 1972), indicating a drop in pressure. The presence of fine intergrowth of spinel and cordierite around sapphirine is related to the reaction:

$$\text{Sapphirine}_{2:2:1} = \text{spinel} + \text{cordierite}. \quad (12)$$

Cordierite moats between orthopyroxene-sillimanite could be attributed to the following Fe-Mg continuous reaction:

$$\text{Orthopyroxene} + \text{sillimanite} + \text{quartz} = \text{cordierite}. \quad (13)$$

Harris and Holland (1984) have thermodynamically modelled the equilibria (13) which has a gentle positive $\mathrm{d}P/\mathrm{d}T$ slope.

This was followed by the resorption of garnet to give rise to cordierite through the reactions:

$$\text{Garnet} + \text{sillimanite} + \text{quartz} = \text{cordierite}. \quad (14)$$

$$\text{and Garnet} + \text{quartz} = \text{cordierite} + \text{orthopyroxene}. \quad (15)$$

Both these garnet breakdown textures resulting from the continuous reactions (14) and (15) are diagnostic of decompression (e.g., Harley 1989).

Abundant fine grained symplectites of (Cd + Qz+ Kf + Opx), possibly replacing former osumilite, could be ascribed to the reaction:

$$\text{Osumilite} = \text{cordierite} + \text{quartz} + \text{K-feldspar} + \text{orthopyroxene}. \quad (16)$$

Although the exact position of the symplectite producing reactions remains to be determined, the recent experimental data for osumilite stability provides far better P-T constraints (Motoyoshi *et al* 1993; Audibert *et al* 1995; Carrington and Harley 1995).

In this way, the reaction history during sapphirine-cordierite stage, wherein cordierite-forming reactions are evident in a variety of textures, is characterized by decompression. Prisms of corundum included in the exsolved magnetite-spinel association could be related to an oxidation reaction (e.g., Waters 1991):

$$\text{Hercynite} + O_2 = \text{magnetite} + \text{corundum}. \quad (17)$$

5.3 *Retrogressive hydration reactions*

Finally, during the late hydration stage, retrogression of garnet, orthopyroxene and cordierite is evidenced from the occurrence of biotite, fine sillimanite intergrown with biotite or biotite + quartz symplectites. The main retrogressive hydration reactions are as follows.

$$\text{Orthopyroxene} + \text{K-feldspar} + \text{V} = \text{biotite} + \text{quartz}. \quad (18)$$

$$\text{Garnet} + \text{K-feldspar} + \text{V} = \text{biotite} + \text{sillimanite} + \text{quartz}. \quad (19)$$

$$\text{Cordierite} + \text{K-feldspar} + \text{V} = \text{biotite} + \text{sillimanite} + \text{quartz}. \quad (20)$$

$$\text{Cordierite} + \text{orthopyroxene} + \text{K-feldspar} + \text{V} = \text{biotite} + \text{quartz}. \quad (21)$$

There is a possibility that some of these textures could have been produced by melt-solid back reactions.

6. Estimation of *P-T* conditions

An attempt is made to quantify the P-T evolution of the sapphirine granulites. Attainment of mosaic equilibrium on textural grounds between the phases in question is the basic yardstick for the application of geothermobarometry. Metamorphic conditions are calculated using the conventional geothermobarometers as well as thermodynamically calibrated MAS equilibria. The sapphirine granulites described here are suitable for the application of thermobarometry because most of the solid–solid reactions involve large volume changes and hence they should be robust to attached uncertainties. Relevant reaction calibrations with their activity functions taken from Lal (1997) are summarized in the Appendix. These calibrations were applied to core and rim compositions. It is now apparent that even Fe-Mg exchange thermometry on

most refractory phases (e.g., garnet-orthopyroxene core compositions) in grain contact may not record peak conditions due to resetting (Pattison and Begin 1994 and the references therein). Therefore, P-T estimates were also obtained from distant mineral grains that are within the domain of textural equilibrium (e.g., garnet with highest X_{Mg} and orthopyroxene with maximum Al_2O_3 contents). This can usually be assessed by comparing the compositions of several grains in the rock. Selection of such mineral points should possibly minimize reequilibration effects. On the basis of the intersection of equilibria, we obtain P and T estimates for the rock (table 3) which may not be without uncertainties associated with a-x relations of the phases involved. Core compositions of garnet, orthopyroxene, and other cordierite-absent phases yield higher pressure values c. 8.4 kbar in the temperature range of 865–910°C (figure 4a). This estimate is consistent with minimum temperature constraints imposed by the high Al_2O_3 contents of orthopyroxene (c. 9.0 wt%) coexisting with sillimanite ± quartz or sapphirine + quartz association. It was followed by the cordierite stage which records a systematic decrease in the pressure estimates with a minimum pressure of 5.4 kbar at c. 750°C. The apparent pressure difference between the cordierite-absent and the cordierite-bearing assemblages is also in agreement with the FMAS and KFMASH petrogenetic grids for high fO_2 of Hensen (1986) and Dasgupta *et al* (1995) respectively, wherein late cordierite overprinting clearly reflects decompression.

The calculated P-T conditions characterize a decompression of c. 3 kbar as well as moderate cooling

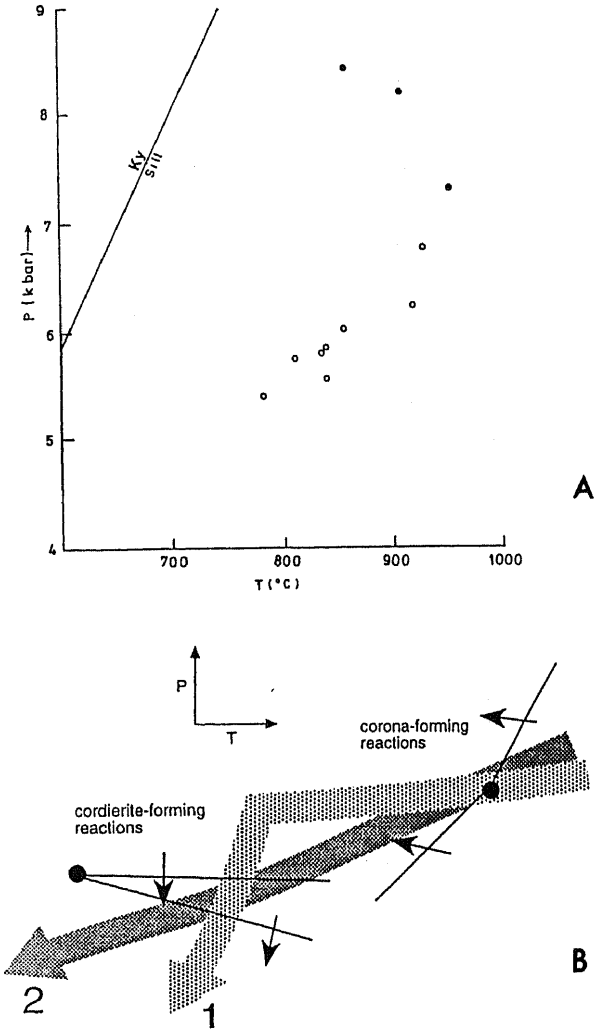

Figure 4(**A**). Pressure-temperature values for the sapphirine granulites of the present area obtained from the intersection of the different mineral equilibria (see table 3). Solid circles represent cordierite-absent equilibria and open circles refer to cordierite-bearing equilibria. (**B**) Orientations for the corona-forming reactions and for the cordierite-forming reactions in P-T space. The small arrows indicate the direction that these reactions would proceed and the large arrows depict the two possible P-T paths.

Table 3. *P-T estimates for sapphirine granulite.*

Sample no.	Reactions involved*	P (kbar)	T (°C)
R93/80	2, 4, 5, 6, 7	8.4	865
	2, 4, 5, 6, 7	8.2	910
	1, 3, 7	7.3	955
	2, 11, 12, 13	6.8	960
	7, 10, 13, 14	6.0	860
	7, 10, 13, 14	5.8	810
	8, 9, 10	5.4	780
R93/59	7, 10, 13, 14	5.8	840
	2, 11, 12, 13	5.8	835
R93/61	7, 10, 13, 14	6.3	920

* (1) Gt = Opx + Sill + Sp; (2) Opx + Sill = Gt + Qz.
(3) Sp + Qz = Gt + Sill; (4) Opx + Sill + Sa = Gt.
(5) Sa + Qz = Gt + Sill; (6) Opx + Sa + Qz = Gt.
(7) Sa + Qz = Opx + Sill; (8) Sp + Cd = Sa.
(9) Sp + Cd = Opx + Sill; (10) Sa + Cd = Opx + Sill.
(11) Gt + Qz + Sill = Cd; (12) Gt + Qz = Opx + Cd.
(13) Opx + Sill + Qz = Cd; (14) Sa + Qz = Cd.
For thermobarometric calibrations of these reactions refer to Appendix.

(up to 200°C). However, the decompression is not isothermal or near-isothermal. Independent P-T estimates were also obtained using the garnet-cordierite-sillimanite-quartz equilibrium ($n = 2$). Of the several formulations for this equilibria we have chosen the models of Thompson (1976), Perchuk (1991) and Bhattacharya *et al* (1988). The calculated P-T vectors give consistently lower values of temperature and pressure (table 4). The P-T conditions constrained by garnet-orthopyroxene-plagioclase-quartz equilibria for the charnockites yield lower estimates of 6.3 kbar at an average temperature of 740°C (table 5). Wide ranging P-T conditions determined for the E. Ghats granulites have been reviewed recently by Sen *et al* (1995).

Table 4. *Estimated temperature (°C) and pressure (kbar) using Gt-Cd-Sill-Qz thermobarometry.*

References/ Sample nos.	T	P	B	
R93/80(C)	744–748	721–724	692–694	T
($n = 2$)	6.5–6.6	8.3		P_{Mg}
	7.2–7.3		6.3–6.4	P_{Fe}
R93/59(R)	652–658	643–648	653–657	T
($n = 2$)	6.2	7.9		P_{Mg}
	7.7–7.8		6.9	P_{Fe}

Calculation at 8 kbar/800°C, T: Thompson (1976), P: Perchuk (1991), B: Bhattacharya *et al* (1988).

Table 5. *Estimated temperature (°C) and pressures (kbar) using Gt-Opx-Plag-Qz thermobarometry.*

References/ Sample nos.	SB	H	B	L	
R93/92	766–776	698–705	742–751	732–745	T
($n = 2$)			6.4	7.3	P_{Mg}
	7.2–7.3		6.4	7.2	P_{Fe}

Calculation at 8 kbar/800°C, H: Harley (1984), SB: Sen and Bhattacharya (1984), B: Bhattacharya *et al* (1991); L: Lal (1993).

7. Tectonic significance of metamorphic history

From the interpretation of textural history, there seems to be evidence of an initial stage of reaction textures consistent with cooling (the corona stage), followed by a stage of reaction textures consistent with decompression (the cordierite stage). This could be explained in terms of two different P-T paths (figure 4b): (i) a path with initial cooling segment, followed by a decompression-dominated segment; (ii) a retrograde path with a moderate dP/dT to cross both the corona-forming reactions and the cordierite-forming reactions. However, it has not been possible to determine the sequence of cordierite-absent reactions with respect to time. Thus it is likely that these cordierite-absent reactions with a narrow P-T range may have formed close to [Cd] invariant point. Therefore, a retrograde P-T path with moderate dP/dT slope would explain both the corona-forming and cordierite-forming reactions in the P-T space.

The reaction textures in the study area developed during decompression represents the post-peak segment of the P-T path. P-T vectors from granulite facies rocks in the G. Madugula area indicate that the rocks experienced substantial decompression (up to 3 kbar) and moderate cooling (150–200°C) subsequent to the peak conditions of metamorphism. Such a P-T vector is not uncommon in granulite facies terranes and similar retrograde decompressive P-T paths have been reported from several localities including southern India and the Eastern Ghats (Droop and Bucher-Nurminen 1984; Windley *et al* 1984; Chacko *et al* 1987; Lal *et al* 1987; Currie and Gittins 1988; Droop 1989; Harley *et al* 1990; Clarke and Powell 1991; Mengel and Rivers 1991; Kihle and Bucher-Nurminen 1992; Mohan and Windley 1993; Dasgupta *et al* 1994). The majority of the workers in different areas of E. Ghats have documented the retrograde trajectory subsequent to the peak metamorphic conditions but Sengupta *et al* (1990) have attempted to suggest a qualitative prograde path shown by dashed lines. A multi-stage P-T record from Chilka area and a high T decompression path with the structural evidence of an early compressional regime (Sen *et al* 1995), opens up possibility of clockwise P-T path in agreement with the conclusions reached by Lal *et al* (1987) and Dasgupta *et al* (1994). In the present study, the textural history and geothermobarometry appear to reflect a decompressional P-T trajectory which may be ascribed to a setting dominated by exhumation after crustal thickening. The exhumation mechanism, however, remains uncertain. Tectonic models for granulite formation which take into account the decompressive P-T path include (i) crustal thickening due to collisional models (Thompson and England 1984); (ii) an extensional regime involving a crust of near-normal thickness (Sandiford and Powell 1986). Calculated peak P-T conditions suggest that the G. Madugula sapphirine granulites were buried to depths of c. 28 km. The crustal thickness beneath the E. Ghats is now c. 35 km (Kalia *et al* 1979); if it can be demonstrated that this subjacent crust underlay the investigated area at the time of metamorphism and has not been thickened by subsequent shortening or magmatic underplating; then the total crustal thickness may have been as much as c. 65 km. Such a profound crustal thickness could be possibly generated by collision tectonics. Discrimination between these tectonic models is also hindered mainly by a lack of data on cooling history and inadequate systematic isotopic age data in the E. Ghats belt. Nonetheless, we suggest that the choice of an appropriate model must take into account the petrological findings presented in this study for a decompressive history. Whether these assemblages developed in a single metamorphic event or represent two or more unrelated events overprinting one another is still a matter of debate until more age data for different sectors of Eastern Ghats belt becomes available.

Acknowledgements

We thank Professor S K Sen for his invitation to write this paper and his subsequent patience for a late contribution. Discussions and numerous helpful suggestions with Professor R K Lal are deeply appreciated.

Constructive criticism by Dr. I Fitzsimons and Dr. S Dasgupta are gratefully acknowledged. This work was supported by the Department of Science and Technology Project Grant to Dr. A Mohan. This work is a contribution to the IGCP 304 and 368 projects.

APPENDIX

Relevant reaction calibration and their activity functions.

1. $P = 1 + [T(R\ln K_D - 3.030) + 15920]/(0.9706)]$;
   $K_D = X^4_{Py}/X^5_{Ens} \cdot X^2_{Sp}$.
2. $P = 1 + [T(-4.47 - R\ln K_D) + 11080]/(0.3587)$;
   $K_D = X^3_{Ens}/X^2_{Py}$.
3. $P = 1 + [T(6.63 + R\ln K_D) - 3820]/(0.559)$;
   $K_D = X_{Py}/X^3_{Sp}$.
4. $P = 1 + [T(0.655 + R\ln K_D) + 9400]/(0.6959)$;
   $K_D = X^3_{Py}/X_{Sa} \cdot X^{3.5}_{Ens}$.
5. $P = 1 + [T(17.61 + R\ln K_D) - 10580]/(0.8320)$;
   $K_D = X^2_{Py}/X^3_{Sa}$.
6. $P = 1 + [T(2.89 + R\ln K_D) + 3860]/(0.5165)$;
   $K_D = X^2_{Py}/X_{Sa} \cdot X^2_{Ens}$.
7. $T = [0.157744(P - 1) + 7220]/(7.36 + R\ln K_D)$;
   $K_D = X_{Ens}/X_{Sa}$.
8. $P = 1 + [T(-4.93 - R\ln K_D) + 10190]/(1.3129)$;
   $K_D = X^8_{Sp} \cdot X_{Cd}/X^5_{Sa}$.
9. $P = 1 + [T(38.83 - R\ln K_D) - 10040]/(4.6097)$;
   $K_D = X^4_{Cd} \cdot X^2_{Sp}/X^5_{Ens}$.
10. $P = 1 + [T(32.05 - R\ln K_D) - 10070]/(3.4252)$;
    $K_D = X_{Sa} \cdot X^3_{Cd}/X^4_{Ens}$.
11. $P = 1 + [T(20.22 - R\ln K_D) + 8230]/(3.6262)$;
    $K_D = X^3_{Cd}/X^2_{Py}$.
12. $P = 1 + [T(3.76 - R\ln K_D) + 10130]/(1.4479)$;
    $K_D = X^2_{Ens} \cdot X_{Cd}/X^2_{Py}$.
13. $P = 1 + [T(8.23 - R\ln K_D) - 950]/(1.089)$;
    $K_D = X_{Cd}/X_{Ens}$.
14. $P = 1 + [T(0.87 - R\ln K_D) + 6270]/(0.9314)$;
    $K_D = X_{Cd}/X_{Sa}$.

$X_{Cd} = (X^{Cd}_{Mg})^2$, $X_{Py} = (X^{Gt}_{Mg})^3$, $X_{Ens} = (X^{M1}_{Mg} \cdot X^{M2}_{Mg})$, $X_{Sp} = X_{Mg} \cdot X^2_{Al}$.

$X_{Sa_{221}} = X^2_{Mg} \cdot X^4_{Al} \cdot X_{Si}$, where $X_{Si} = Si$ (ten oxygen basis).

$X_{Sa_{793}} = X^7_{Mg} \cdot X^{18}_{Al}$.

$X^{Sa/Sp}_{Al} = Al/(Al + Fe^{+3} + Cr + Ti)$, P in bars, T in Kelvin.

References

Aftalion H, Bowes D R, Dash B and Dempster J J 1988 Late Proterozoic charnockites in Orissa, India: A U-Pb and Rb-Sr isotopic study; *J. Geol.* **11** 663–676

Arima M and Barnett R L 1984 Sapphirine bearing granulites from the Sipiwesk Lake area of the Late Archean Piturtonei granulite terrain, Manitoba, Canada; *Contrib. Mineral. Petrol.* **88** 102–112

Armbruster T and Bloss F D 1980 Channel CO_2 in cordierite; *Nature* **286** 140–141

Audibert N, Hensen B J and Bertrand P 1995 Experimental study of phase relationships involving osumilite in the system K_2O-FeO-MgO-Al_2O_3-SiO_2-H_2O at high pressure and high temperature; *J. Metamorphic Geol.* **13** 331–344

Berg J H R and Wheeler E P II 1976 Osumilite of deep-seated origin in the contact aureole of the anorthositic Nain complex, Labrador; *Am. Mineral.* **61** 29–37

Bertrand P, Ouzegane Kh and Kienast J R 1992 *P-T-X* relationships in the Precambrian Al-Mg-rich granulites from in Ouzzal, Moggar, Algeria; *J. Metamorphic Geol.* **10** 17–31

Bhattacharya A, Mazumdar A C and Sen S K 1988 Fe-Mg mixing in cordierite; constraints from natural data and implication for cordierite-garnet geothermometry to granulites; *Am. Mineral.* **73** 338–344

Bhattacharya A, Krishnakumar K R, Raith M and Sen S K 1991 An improved set of a-x parameter for Fe-Mg-Ca garnet and refinement of the opx-gt thermometer and the opx-gt-plag-qtz barometer; *J. Petrol.* **32** 629–656

Bohlen S R and Essene E J 1977 Feldspar and oxide thermometry in the Adirondack Highlands; *Contrib. Mineral. Petrol.* **62** 153–169

Carrington D P and Harley S L 1995 The stability of osumilite in metapelitic granulites; *J. Metamorphic Geol.* **13** 613–625

Chacko T, Ravindra Kumar G R and Newton R C 1987 Metamorphic *P-T* conditions of the Kerala (S. India) Khondalite Belt: A granulite facies supracrustal terrain; *J. Geol.* **95** 343–358

Chatterjee N D and Schreyer W 1972 The reaction enstatite$_{ss}$+ sillimanite = sapphirine$_{ss}$+ quartz in the system MgO-Al_2O_3-SiO_2; *Contrib. Mineral. Petrol.* **36** 49–62

Clarke G L and Powell R 1991 Decompressional coronas and symplectites in granulites of Musgrave Complex, Central Australia; *J. Metamorphic Geol.* **9** 441–450

Currie K L and Gittins J 1988 Contrasting sapphirine parageneses from Wilson Lake, Labrador and their tectonic implications; *J. Metamorphic Geol.* **6** 603–22

Dasgupta S, Sanyal S, Sengupta P and Fukuoka M 1994 Petrology of Granulites from Anakapalle-Evidence for Proterozoic Decompression in the Eastern Ghats, India; *J. Petrol.* **35** 433–459

Dasgupta S, Sengupta P, Ehl J, Raith M and Bardhan S 1995 Reaction texture in a suite of spinel granulite from the Eastern Ghats belt, India: Evidence for polymetamorphism a partial petrogenetic grid in the system KFMASH and the roles of ZnO and Fe_2O_3; *J. Petrol.* **36** 435–461

Droop G T R 1989 Reaction history of garnet sapphirine granulites and conditions of Archean high-pressure granulite facies metamorphism in central Limpopo mobile belt, Zimbabwe; *J. Metamorphic Geol.* **7** 383–403

Droop G T R and Bucher-Nurminen K 1984 Reaction textures and metamorphic evolution of sapphirine-bearing granulites from the Gruf complex, Italian Central Alps; *J. Petrol.* **25** 766–803

Ellis D J, Sheraton J W, England R N, Dallwitz W B 1980 Osumilite-sapphirine-quartz granulites from Enderby Land, Antarctica-Mineral assemblages and reactions; *Contrib. Mineral. Petrol.* **74** 201–10

Grew E S 1982a Sapphirine-Kornerupine and sillimanite + orthopyroxene in the charnockitic region of south India; *J. Geol. Soc. India* **23** 469–505

Grew E S 1982b Osumilite in the sapphirine quartz terrane of Enderby Land, Antarctica: Implications for osumilite petrogenesis in the granulite facies; *Am. Mineral.* **67** 762–87

Grew E S and Manton W I 1986 A new correlation of sapphirine granulites in the Indo-Antarctic metamorphic terrain: Late Proterozoic dates from the Eastern Ghats; *Precam. Res.* **33** 123–39

Hamm H W and Vieten K 1971 Zur Berechnung der kristall-Chemischen Formel und des Fe^{3+}-Genaltes von Klinopyroxenen aus Elektronenstrahl-Mikroanalysen; *N. Jb. Miner. Mh.* 310–14

Harley S L 1984 An experimental study of the partitioning of Fe and Mg between garnet and orthopyroxene; *Contrib. Mineral. Petrol.* **86** 359–373

Harley S L 1989 The origin of granulites: A metamorphic perspective; *Geol. Mag.* **126** 215–47

Harley S L, Hensen B J and Sheraton J W 1990 Two stage decompression in orthopyroxene-sillimanite granulites from Forefinger Point Enderby Land Antarctica: Implications for the evolution of the Archean Napier Complex; *J. Metamorphic Geol.* **8** 591–613

Harris N B W and Holland T J B 1984 The significance of cordierite-hypersthene assemblages from the Beilbridge region of the central Limpopo belt, evidence for rapid decompression in the Archean; *Am. Mineral.* **69** 1036–1049

Hensen B J 1986 Theoretical phase relation involving cordierite and garnet revisited the influence of oxygen fugacity on the stability of sapphirine and spinel in the system Mg-Fe-Al-Si-O; *Contrib. Mineral. Petrol.* **92** 362–367

Higgins J B, Ribbe P H and Herd R K 1979 Sapphirine I: Crystal chemical contributions; *Contrib. Mineral. Petrol.* **68** 349–56

Kalia K L, Roy Chowdhury K, Reddy P R, Krishna V G, Narain H, Subbotin S I, Sollugub V B, Chekunov A V, Kharetchko G E, Lazarenk O M A and Ilchenko T V 1979 Crustal structure along Karali-Udipi profile in the Indian peninsular shield from deep seismic sounding; *J. Geol. Soc. India* **20** 307–33

Kamineni D C and Rao A T 1988a Sapphirine granulites from Kakanuru area, Eastern Ghats, India; *Am. Mineral.* **73** 692–700

Kamineni D C and Rao A T 1988b Sapphirine-bearing quartzite from the Eastern Ghats granulites terrains, Vizianagaram India; *J. Geol.* **96** 209–220

Kihle J and Bucher-Nurminen K 1992 Orthopyroxene-sillimanite Sapphirine granulites from the Bamble granulite terrane, Southern Norway; *J. Metamorphic Geol.* **10** 671–683

Lal R K 1993 Internally consistent recalibrations of mineral equilibria for geothermobarometry involving garnet-orthopyroxene-plagioclase-quartz assemblage and their application to the south Indian granulites; *J. Metamorphic Geol.* **11** 855–866

Lal R K 1997 Internally consistent calibrations for geothermobarometery of high-grade Mg-Al rich rocks in the system MgO-$Al_2O_3SiO_2$ and their application to sapphirine-spinel granulites of Eastern Ghats, India and Enderby Land, Antarctica; this volume, pp. 91–113

Lal R K, Ackermand D and Upadhyay H 1987 *P-T-X* relationships deduced from corona textures in sapphirine-spinel-quartz assemblages from Paderu Southern India; *J. Petrol* **28** 1139–1168

Mengel F Z and Rivers T 1991 Decompression reactions and *P-T* conditions in High grade Rocks, Northern Labrador *P-T-t* paths from individual samples and implications for Early Proterozoic Tectonic Evolution; *J. Petrol.* **32** 139–167

Mohan A and Windley B F 1993 Crustal trajectory of sapphirine-bearing granulites from Ganguvarpatti, South India: evidence for an isothermal decompression path; *J. Metamorphic Geol.* **11** 867–878

Motoyoshi Y, Hensen B J and Arima M 1993 Experimental study of the high pressure stability limit of osumilite in the system K_2O-MgO-Al_2O_3-SiO_2 implications for high-temperature granulites; *Eur. J. Mineral.* **5** 439–445

Newton R C 1972 An experimental determination of the high-pressure stability limits of magnesium cordierite under wet and dry conditions; *J. Geol.* **80** 398–420

Paul D K, Ray Barman T, McNaughton N J, Fletcher I R, Potts P J, Ramakrishna M and Augustive P F 1990 Archean-Proterozoic evolution of Indian charnockite: Isotopic and geochemical evidence from granulite of the Eastern Ghats belt; *J. Geol.* **98** 253–263

Perchuk L L 1991 Derivation of a thermodynamically consistent set of geothermometers and geobarometers for metamorphic and magmatic rock. In: *Progress in metamorphic and magmatic petrology; A memorial volume in honour of D S Korzhinskiy* (ed) L L Perchuk (Cambridge University Press) Chapter 5 93–111

Pattison D R M and Begin N J 1994 Zoning pattern in orthopyroxene and garnet in granulites: Implication for geothermobarometry; *J. Metamorphic Geol.* **12** 387–410

Sandiford M and Powell R 1986 Deep crustal metamorphism during continental extension: Modern and ancient examples; *Earth Planet. Sci. Lett.* **79** 151–158

Sen S K and Bhattacharya A 1984 An orthopyroxene-garnet thermometer and its application to the Madras charnockites; *Contrib. Mineral. Petrol.* **88** 64–71

Sen S K, Bhattacharya S and Acharyya A 1995 A multistage pressure-temperature record in Chilka Lake granulites: The epitome of the metamorphic evolution of Eastern Ghats, India; *J. Metamorphic Geol.* **13** 287–298

Sengupta P, Dasgupta S, Bhattacharya P K, Fukuoka M, Chakraborti S and Bhowmick S 1990 Petro-tectonic imprints in the sapphirine granulites from Anantagiri, Eastern Ghats mobile belt India; *J. Petrol.* **31** 971–996

Thompson A B 1976 Mineral reaction in pelitic rocks calculation of some *P-T-X* (Fe-Mg) phase relations; *Am. J. Sci.* **276** 425–454

Thompson A B and England P C 1984 Pressure-temperature-time paths of regional metamorphism II. Their inference and interpretation using mineral assemblages in metamorphic rocks; *J. Petrol.* **25** 929–55

Waters D J 1991 Hercynite-quartz granulites. Phase relations and implications for crustal processes; *Eur. J. Mineral.* **3** 367–386

Windley B F, Ackermand D and Herd R K 1984 Sapphirine/Kornerupine-bearing rocks and crustal uplift history of the Limpopo belt, Southern Africa; *Contrib. Miner. Petrol.* **86** 342–358